Artificial Ground Freezing of Fully Saturated Soil: Thermal Problem

Roman Lackner[1]; Andreas Amon[2]; and Hannes Lagger[3]

Abstract: Freezing of water in porous media such as soil results in a change of mechanical and thermal properties. This change of properties is exploited during artificial ground freezing (AGF) employed in tunneling, during open excavations, and for retaining structures. In this paper, a phase-change model for the simulation of freezing of fully saturated soil is presented. Disregarding the influence of mechanical loading on the freezing process, only the solution of the thermal problem, i.e., determination of the temperature field, is addressed. The (macroscopic) thermal properties are related to the material parameters of the different material phases, such as soil particles, water, and ice. This approach allows us to minimize the number of input parameters of the phase-change model and to account for the change of thermal properties in the course of the freezing process. The performance of the proposed model is illustrated by the reanalysis of freezing experiments and of an AGF construction site in Vienna, Austria.

DOI: 10.1061/(ASCE)0733-9399(2005)131:2(211)

CE Database subject headings: Frozen soils; Freezing; Homogeneity; Soil improvement; Tunneling; Saturated soils; Thermal analysis.

Introduction—Physics of Freezing

Nucleation and Crystal Growth in Water

Freezing of water is initiated at temperatures below the freezing temperature T_f by unstable clusters of water molecules (Shackelford 2000). The driving force of this liquid-phase instability is a function of $T-T_f$ and increases with decreasing temperature [see Fig. 1(a)]. In general, the freezing temperature T_f itself depends on structural imperfections in the liquid such as foreign surfaces. Whereas T_f equals approximately $-40\,^\circ$C for pure water (Fletcher 1970), the large number of heterogenities providing foreign surfaces in soils results in an increase of T_f to $0\,^\circ$C.

In the course of ice formation, the liquid-phase instability is followed by the diffusion of adjacent water molecules toward the formed cluster in order to form small nuclei of ice crystals [see Fig. 1(b)]. This continuous increase is essential for the formation of stable nuclei which are characterized by a radius larger than the critical radius. Nuclei with a radius smaller than the critical radius might fall back to the liquid phase.

Both processes the liquid-phase-instability and the local diffusion process are parts of the so-called nucleation process. Accordingly, the driving force of the nucleation process consists of the driving force of liquid-phase instability and an Arrhenius term (Atkins 1994) accounting for the local diffusion process, reading

$$\text{nucleation rate} = \alpha(T_f - T)^\beta A_n \exp\left(-\frac{Q_n}{RT}\right) \tag{1}$$

where α and β = constant parameters; A_n and Q_n = pre-exponential constant and the activation energy for the local diffusion process, respectively; R = universal gas constant; and T = absolute temperature.

If a nucleus has reached the critical radius, crystal growth takes place [see Fig. 1(c)]. The diffusion of water molecules controls the crystal growth, described by an Arrhenius expression in the form

$$\text{growth rate} = A_g \exp\left(-\frac{Q_g}{RT}\right) \tag{2}$$

where A_g and Q_g = pre-exponential constant and the activation energy of the crystal growth.

The overall transformation rate from the liquid phase to the solid phase is obtained as the product of the nucleation rate (1) and the growth rate (2).

Enthalpy of Phase Change

When water freezes, the previously free and moving water molecules become arranged within the fixed crystal structure of the ice. This reduction of movement ability results in a decrease of the enthalpy H. The enthalpy change of freezing is equal to $\Delta H = -334$ kJ/(kg water) (Atkins 1994). Since the enthalpy is re-

[1]University Dozent, Institute for Mechanics of Materials and Structures, Vienna Univ. of Technology, Karlsplatz 13/202, A-1040 Vienna, Austria. E-mail: roman.lackner@tuwien.ac.at

[2]Geotechnical Engineer, Geoconsult (GC), Asia Sinapore PTE Ltd., 100 Beach Rd., 17-08/09 Shaw Tower, Singapore 189702; formerly, Student, Vienna Univ. of Technology, Vienna, Austria. E-mail: andreas.amon@geoconsult.com.sg

[3]Senior Tunnel Engineer, Ove Arup and Partners, 155 Avenue of the Americas, New York, NY 10013; formerly, Student, Vienna Univ. of Technology, Vienna, Austria. E-mail: hannes.lagger@arup.com

Note. Associate Editor: Jin Y. Ooi. Discussion open until July 1, 2005. Separate discussions must be submitted for individual papers. To extend the closing date by one month, a written request must be filed with the ASCE Managing Editor. The manuscript for this paper was submitted for review and possible publication on September 17, 2002; approved on February 3, 2004. This paper is part of the ***Journal of Engineering Mechanics***, Vol. 131, No. 2, February 1, 2005. ©ASCE, ISSN 0733-9399/2005/2-211–220/$25.00.

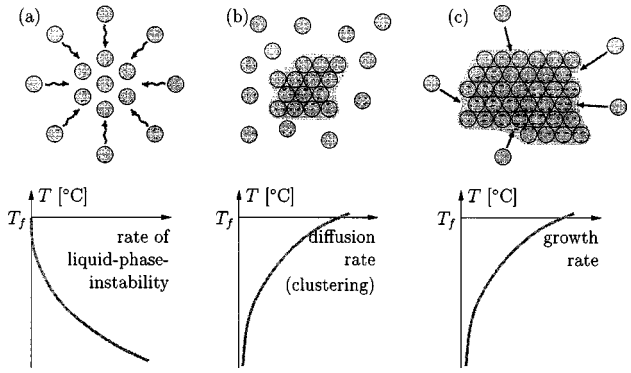

Fig. 1. Nucleation and crystal growth: (a) clustering of adjacent molecules to form (b) crystalline nucleus followed by (c) growth of crystalline phase

duced during freezing, heat is released rendering freezing as an exothermal process, with a released energy of 334 kJ/(kg water).

Freezing in Porous Media

In porous media, some water is bound to the surface of the particles by means of chemical bonds and electrostatic forces. The binding is the strongest at the particle surface and decreases with increasing distance to the binding level of free water. Freezing of water in porous media begins where the level of binding is the lowest, i.e., in the middle of the pores and proceeds progressively toward the pore walls. However, even at temperatures below the freezing temperature, a water layer around the particles remains unfrozen. The thickness of this layer depends on the above-mentioned chemical bonds and electrostatic forces, and the temperature. For continuously decreasing temperatures, the thickness of the layer of unfrozen water decreases. Fig. 2 shows the amount of unfrozen water, given by the difference of the water content of the unfrozen soil w and the frozen water content w_f, as a function of the temperature T for different types of soil. For clay which is characterized by the largest specific surface the unfrozen water content is the largest.

Even for temperatures significantly lower than the freezing temperature, i.e., for $T \ll T_f$, a layer of water remains unfrozen. The respective amount of unfrozen water is given by $w - w_{f,\infty}$, where $w_{f,\infty}$ is the final frozen water content, with $w_{f,\infty} < w$. In general, $w_{f,\infty}$ depends on the water content w, the specific surface area of the soil, and the binding at the particle surfaces. The introduction of $w_{f,\infty}$ allows the definition of a degree of freezing ξ in the form

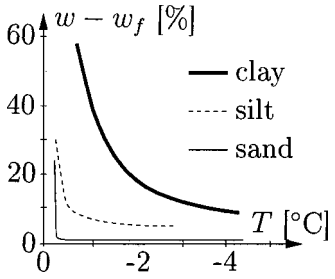

Fig. 2. Unfrozen water content $w-w_f$ as function of T for different types of soil (Willams 2001) (w: water content of unfrozen soil; w_f: frozen water content)

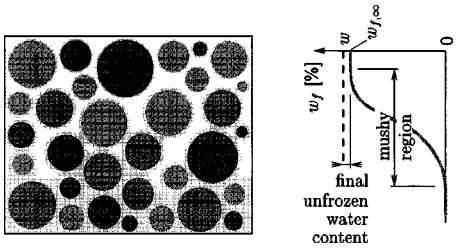

Fig. 3. Illustration of mushy region in freezing of porous media

$$\xi = \frac{w_f}{w_{f,\infty}} \text{ with } 0 \leq \xi \leq 1 \tag{3}$$

Whereas for $\xi = 0$, no freezing has occurred, $\xi = 1$ is characterized by a frozen water content having reached its final value $w_{f,\infty}$. Regions characterized by $0 < \xi < 1$ are commonly referred to as mushy regions (see Fig. 3).

The evolution of the degree of freezing is described by the freezing rate ξ°, such that $\xi^\circ dt$ is the amount of ice per unit volume formed during time interval dt of the freezing process. In the case of a closed system with regard to the water phase, $\xi^\circ = d\xi/dt$. In general, however, water flow results in a change of the water content w and, hence, of the final unfrozen water content $w_{f,\infty}$. In that case, ξ° cannot be presented by the time derivation $d\xi/dt$ (Coussy 1995).

In the following, a phase-change model for the simulation of freezing in porous media will be presented. In contrast to models focusing on the solution of the so-called Stefan problem, where the heat transfer of one single material experiencing phase change is considered (see, e.g., Rolph and Bathe 1982), the interaction between the material being subjected to phase change (water) and the inclusions (soil particles) will be taken into account.

Phase-Change Model

The phase-change model presented in this section allows the description of freezing of fully saturated soil, where the movement of pore water is not taken into account (closed system). Accordingly, the water content w of the unfrozen soil, and hence $w_{f,\infty}$, are constant and become soil-specific quantities. For a constant value of $w_{f,\infty}$, the degree of freezing ξ defined in Eq. (3) uniquely represents the state of the freezing process as a function of the frozen water content w_f. Accordingly, the freezing rate ξ° can be replaced by $\dot{\xi}$, with $\dot{\xi} = d\xi/dt$.

Freezing Kinetics

The freezing rate $\dot{\xi}$ is given by the product of the nucleation rate and the growth rate [see Eqs. (1) and (2)]. Introducing $Q = Q_n + Q_g$ and $A = \alpha(T_f - T)^\beta A_n A_g$, $\dot{\xi}$ becomes

$$\dot{\xi} = \alpha(T_f - T)^\beta A_n A_g \exp\left(-\frac{Q_n + Q_g}{RT}\right) = A \exp\left(-\frac{Q}{RT}\right) \tag{4}$$

Considering a linearly decreasing function for $A(\xi)$, with $A = A_0(1-\xi)$, where $A_0 = A_0(T)$, in Eq. (4) yields a differential equation for the degree of freezing ξ. For a constant temperature $\overline{T}$, an explicit form for the characteristic time for the freezing process can be extracted from the solution of this differential equation

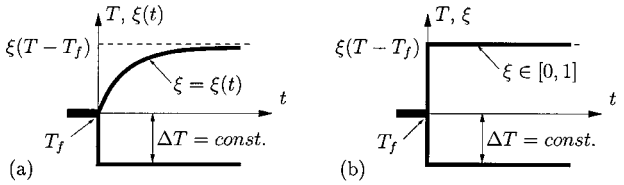

Fig. 4. Illustration of freezing kinetics: evolution of ξ: (a) obtained from linearly decreasing chemical affinity function and (b) adopted in proposed material model

$$\tau_f = \left[A_0 \exp\left(-\frac{Q}{RT} \right) \right]^{-1} \tag{5}$$

Fig. 4(a) illustrates the increase of ξ for a temperature T below the freezing temperature T_f, approaching the value of ξ corresponding to the frozen water content at $T-T_f$ (see Fig. 2, where $T_f=0\,^\circ$C). Since the characteristic time τ_f for the freezing process is significantly shorter than the time scale associated with the transport of heat through the soil, any change in temperature can be considered by an abrupt adaptation of the value of ξ to its value corresponding to the frozen water content at $T-T_f$ [see Fig. 4(b)]. Thus, a unique thermal freezing function with

$$\xi = \xi(T - T_f) \tag{6}$$

is obtained.

Thermal Material Properties

For the solution of the thermal problem, three parameters are required, i.e., the density ρ, the heat capacity c, and the thermal conductivity k. In order to minimize the number of input parameters, ρ, c, and k are related to the properties of the different material phases, such as the soil particles, water, and ice.

1. In contrast to other fluids, the bipolar character of the water molecules results in an increase of the volume during freezing by 9%. The respective decrease of the density ρ [kg/m^3] of the particle–water–ice composite is estimated by the volume average

$$\rho(\xi) = f_p \rho_p + (1 + f_p - f_i)\rho_w + f_i \rho_i \tag{7}$$

   where f_p and $f_i = f_{i,\infty}\xi$ represent the volume fraction for the soil particles and ice, with $f_{i,\infty}$ as the final volume fraction of the ice phase for $T \ll T_f$. In Eq. (7), ρ_p, ρ_w, and ρ_i = densities of the soil particles, water, and ice.
2. With regard to the heat capacity c [kJ/(kg K)], volume averaging is applied to the volumetric heat capacity, given by ρc [kJ/(m^3 K)], reading for the particle–water–ice composite

$$c(\xi) = \frac{1}{\rho}[f_p \rho_p c_p + (1 - f_p - f_i)\rho_w c_w + f_i \rho_i c_i] \tag{8}$$

   where c_p, c_w, and c_i = heat capacities of the soil particles, water, and ice.
3. Finally, an estimate for the thermal conductivity k [kJ/(m h K)] of the three-phase composite is obtained from homogenization employing continuum micromechanics. Considering the soil particles and the ice phase as spherical inclusions embedded in a matrix of water, the thermal conductivity becomes [see Fig. 5(b)] (Hatta and Taya 1986; Lackner et al. 2004)

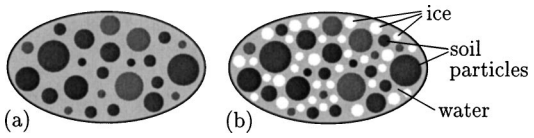

Fig. 5. On determination of thermal conductivity from continuum micromechanics: employed material representation of (a) unfrozen soil and (b) frozen soil

$$k(\xi) = k_w + \frac{\dfrac{f_p(k_p - k_w)}{1 + S(k_p/k_w - 1)} + \dfrac{f_i(k_i - k_w)}{1 + S(k_i/k_w - 1)}}{(1 - f_p - f_i) + \dfrac{f_p}{1 + S(k_p/k_w - 1)} + \dfrac{f_i}{1 + S(k_i/k_w - 1)}} \tag{9}$$

where k_p, k_w, and k_i = thermal conductivities of the soil particles, water, and ice. In Eq. (9), S represents the second-order Eshelby tensor for the thermal problem which, in the case of spherical inclusions, equals 1/3.

Latent Heat of Freezing

In addition to the change of material parameters, phase change causes the release or consumption of energy in the form of latent heat. The latent heat of freezing of water is the quantity of heat released when a unit mass of water is converted into ice. It is given by 334 kJ/(kg water). For a unit volume (1 m^3) of soil, the latent heat of freezing is given by the final volume fraction of ice $f_{i,\infty}$ reading

$$\ell_\xi = 334 \rho_i f_{i,\infty} \ [\text{kJ/(m}^3 \text{ soil)}] \tag{10}$$

Experiments

In order to assess the performance of the phase-change model presented in the previous section, freezing experiments were conducted at Vienna Univ. of Technology, Vienna, Austria. The experiments were performed for fully saturated sand.

Experimental Program

Cylindrical specimens with a height of 0.09 m and a diameter of 0.325 m (see Fig. 6) were stored in a cooling box and subjected to a temperature below the freezing temperature. The bottom surface of the specimen was isolated by means of 0.05 m polystyrene. Accordingly, freezing is initiated at the top surface of the speci-

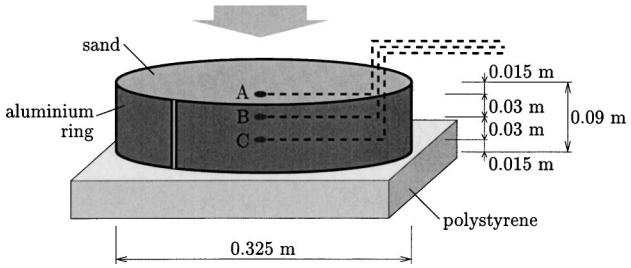

Fig. 6. Freezing experiments: experimental setup and geometric dimensions

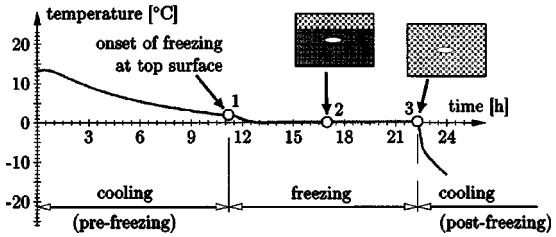

Fig. 7. Freezing experiments: typical temperature history monitored by temperature sensor B

men and the freezing front propagates from the top toward the bottom surface. In order to monitor the temperature evolution in the specimen, three temperature sensors were installed at different distances from the top surface (see Sensors A, B, and C in Fig. 6). Fig. 7 shows a typical temperature history obtained from the temperature sensor in the middle of the specimen (sensor B in Fig. 6). The obtained temperature history can be divided into three parts:

1. Prefreezing period: During this period, the entire specimen is cooled in consequence of the lower temperature in the cooling box. With increasing time, the difference between the box temperature and the specimen temperature at the top surface and, hence, the rate of cooling decreases.
2. Freezing period: The freezing period is initiated by the onset of freezing at the top surface of the specimen (see Point 1 in Fig. 7). The change of thermal properties in consequence of freezing results in an increase of the cooling rate at the location of Sensor B. During the freezing period, the freezing front propagates through the specimen from the top to the bottom surface. Hereby, the release of latent heat prevents the temperature from dropping below T_f.
3. Postfreezing period: When the entire latent heat has been released (see Point 3 in Fig. 7), a rapid decrease of the temperature below the freezing temperature is observed.

Analysis Model

For the reanalysis of the experimental results, a one-dimensional finite element (FE) model is employed, with the orientation of the model coinciding with the axis of the cylindrical specimen. The underlying field equation describing the thermal problem of freezing soil is derived from the first law of thermodynamics, reading

$$\rho(\xi)c(\xi)\dot{T} - \ell_\xi \dot{\xi} = -\operatorname{div} q \tag{11}$$

where ℓ_ξ=latent heat of freezing and q=heat flow. The heat flow q is related to the temperature via a linear heat conduction law (Fourier law), reading

$$q = -k(\xi)\operatorname{grad} T \tag{12}$$

At the top of the soil sample, a radiation-type boundary condition was considered, relating the normal heat flux q_n to the difference between the surface temperature and the temperature in the cooling box T^∞

$$q_n = \alpha(T - T^\infty) \tag{13}$$

with α=radiation coefficient. T^∞ is continuously adjusted to the temperature history measured in the cooling box by an additional temperature sensor.

Table 1. Reanalyses of Experiments: Determination of f_p and $f_{i,\infty}$ for Sand Considered in Experimental Program (Used Material Parameters of Different Material Phases are Listed in Table 2)

Parameter	Value
Mass of saturated soil sample, m	14.76 kg
Mass of soil particles (dried soil sample), m_p	11.64 kg
Mass of water, $m_w = m - m_p$	3.12 kg
Volume of specimen, $V = 0.09 \times 0.325^2\pi/4$	0.007466 m^3
Volume of water, $V_w = m_w/\rho_w$	0.003120 m^3
Volume of soil particles, $V_p = V - V_w$	0.004346 m^3
Volume fraction of water, $f_w = V_w/V$	0.42
Water content, $w = m_w/m_p$	0.27
Final unfrozen water content, $w - w_{f,\infty}$ (Fig. 2)	0.01
Final frozen water content, $w_{f,\infty} = w - (w - w_{f,\infty})$	0.26
Volume fraction of soil particles, $f_p = V_p/V$	0.58
Final volume fraction of ice, $f_{i,\infty} = f_w w_{f,\infty}/w$	0.40

Model Parameters

Thermal Material Properties and Latent Heat of Freezing

The phase-change model presented in the previous section allows us to determine all thermal material properties from two soil-specific quantities only, namely: (1) the volume fraction of the soil particles f_p and (2) the final volume fraction of ice for $T \ll T_f$, $f_{i,\infty}$. The determination of these two parameters for the sand considered in the experimental program is outlined in Table 1. Based on the given values for f_p and $f_{i,\infty}$, and on the thermal properties of the material phases listed in Table 2, the thermal material properties for the unfrozen and frozen soil can be computed as a function of the degree of freezing following Eqs. (7)–(9). The so-obtained material functions are shown in Fig. 8.

The released energy of freezing ℓ_ξ is computed from Eq. (10), employing the final volume fraction of the ice phase $f_{i,\infty}=0.40$ (see Table 1) as ℓ_ξ=121,977 kJ/(m^3 soil).

Thermal Freezing Function

For the simulation of freezing of soil, the thermal freezing function $\xi(T-T_f)$ [see Eq. (6)] has to be specified. At the onset of freezing, i.e., for $T=T_f$, ξ should be equal to zero. Moreover, for $T \ll T_f$, ξ should approach one. A function satisfying the mentioned conditions is given by (see Fig. 9)

Table 2. Reanalyses of Experiments: Thermal Properties of Different Material Phases of Freezing, Saturated Sand and of Polystyrene

Material	ρ [kg/m^3]	c [kJ/(kg K)]	k [kJ/(m h K)]	Reference
Water	1,000	4.2	2.2	(Gröber et al. 1988)
Ice	913	1.9	8.0	(Pitts and Sissom 1977)
Quartz	2,650	0.74	27.7	(Häfner et al. 1992)
Polystyrene	30	1.40	0.14	Manufacturer

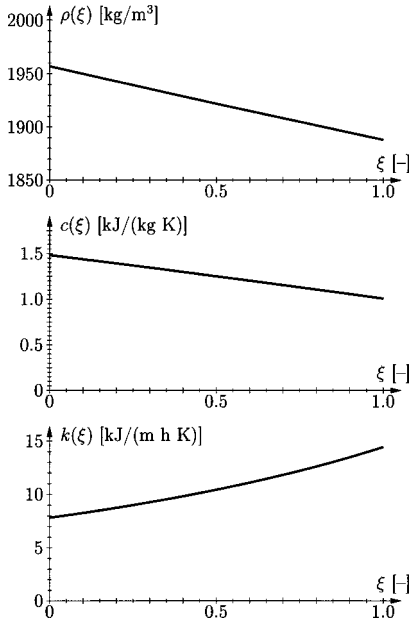

Fig. 8. Freezing experiments: thermal properties for freezing sand as function of ξ

$$\xi(T_f - T) = 1 - \exp\left[- \frac{(T_f - T)^2}{\overline{T}^2} \right] \text{ for } T \leqslant T_f \qquad (14)$$

where $\overline{T}$ = yet unknown calibration parameter. Since the derivative of the thermal freezing function $d\xi/dT$ appears in the second term of field Eq. (11), with $\dot{\xi} = d\xi/dt = d\xi/dT \times dT/dt$, the smoothness of the function depicted in Fig. 9 is essential for the robustness of the employed analysis tool. A similar function was recently proposed for the unfrozen water content by Mikkola and Hartikainen (2002).

Radiation Coefficient

The radiation coefficient (saturated sand–air) α is determined by means of back analysis employing the temperature history of the prefreezing period (see Fig. 7). Hereby, the difference between the measured temperature history and the numerical results is minimized. The temperature curve obtained from the numerical analysis with $\alpha = 300$ kJ/(m² h K) shows excellent agreement between the measured temperature history and the numerical results (see Fig. 10).

Reanalysis of Freezing Experiments

In contrast to the analysis results depicted in Fig. 10, the entire temperature history of the freezing experiment is considered now. During this analysis, the unknown parameter of the thermal freezing function $\overline{T}$ has to be specified. This parameter depends on the specific surface of the considered soil and the chemical bonds and electrostatic forces at the surface of the soil particles. Fig. 11 shows the temperature history obtained from the numerical analysis with $\overline{T} = 0.2\,°\text{C}$. The rather low value for $\overline{T}$ corresponds to the steep decrease of the unfrozen water content of sand with decreasing temperature (see Fig. 2). In the analysis, the change of the radiation coefficient in consequence of freezing is taken into account. The radiation coefficient employed for the frozen soil surface was set equal to $\alpha(\xi = 1) = 85$ kJ/(m² h K). From the obtained numerical results, the following conclusions can be drawn:

1. The time span corresponding to freezing of the specimen (the freezing process is characterized by $T = T_f$) is well predicted by the numerical analysis.
2. When the freezing front reaches the respective temperature sensor, a kink is observed in the numerically obtained temperature history. This kink, however, is not confirmed by the experimental data. This deviation may be caused by local effects arising from the interaction between the temperature sensor and the surrounding soil.
3. In the postfreezing period, good agreement between the numerical results and the experimental data is observed, reflecting the good prediction of the thermal properties of frozen sand by the proposed phase-change model.

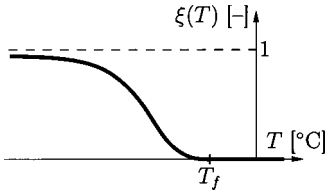

Fig. 9. Thermal freezing function $\xi(T - T_f)$ characterized by $\xi = 0$ at $T = T_f$ and $\xi \to 1$ for $T \ll T_f$

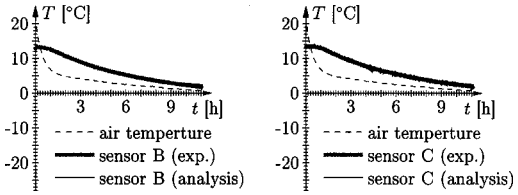

Fig. 10. Freezing experiments: measured temperature histories and results obtained from numerical analysis with $\alpha = 300$ kJ/(m² h K)

Application to Artificial Ground Freezing Construction Site

In this section, the phase-change model is applied to the reanalysis of artificial ground freezing (AGF) performed at a construction site in Vienna. In the course of the construction of the Vienna

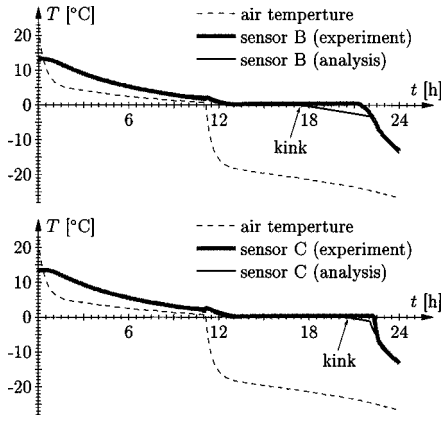

Fig. 11. Freezing experiment: measured temperature histories and results obtained from numerical analysis with $\overline{T} = 0.2\,°\text{C}$ and $\alpha(\xi = 1) = 85$ kJ/(m² h K)

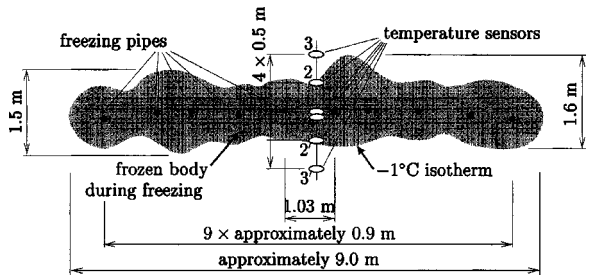

Fig. 12. Application: cross section of test Field V2 showing location of freezing pipes and temperature sensors

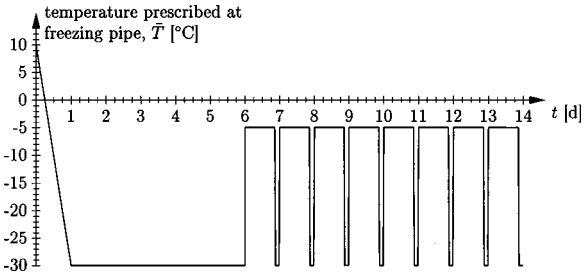

Fig. 14. Application: temperature history in freezing pipe employed in analysis

underground U6, strict ground settlement limitations were set in the area of the TeleCommunication Building (TCB) in order to avoid damage of sensitive installations (Lagger 2001). However, before ground freezing was performed, two test fields, Fields V1 and V2 were frozen, allowing the adaptation of design criteria. These test fields were located in the same soil layer, where freezing beneath the TCB was performed, approximately 6 m below ground level and 1–2 m below the ground water level. In the reanalysis presented in this section, freezing of test Field V2 will be investigated (see Fig. 12). This test field was adjusted with temperature sensors along vertical boreholes in order to monitor the development of the frozen-soil body. The vertical distance between two adjacent temperature sensors was approximately 50 cm (see Fig. 12). The temperature histories at the sensors 1(1′), 2(2′), and 3(3′) are shown in Fig. 13. The observed variations of the temperature histories for sensors characterized by the same distance from the center of the test field are explained by the inaccuracy of the location of the boreholes, the variation of soil properties, and the effect of ground water flow, with a flow velocity of 0.49 m/day (Deix 1992).

The freezing pipes with a diameter of 64 mm were installed in horizontal boreholes. The latter had a diameter of 101.6 mm. The remaining space in the boreholes was filled with cement grout. Altogether ten freezing pipes were employed during freezing of test Field V2. The distance between two adjacent freezing pipes was approximately 0.9 m (see Fig. 12).

A $CaCl_2$ brine was used as cooling material. During soil freezing, the temperature of the brine was reduced to −30°C (the freezing temperature of the brine material itself is −55°C). The freezing process was divided into two parts:

1. During the first 6 days, the brine temperature was decreased to −30°C and kept constant. The purpose of the first part is to build up the frozen-soil body to the required thickness.
2. In the following days, intermittent freezing was performed in order to provide a constant thickness of the frozen-soil body. Hereby, freezing (characterized by a brine temperature of −30°C) was reduced to 3 h/day. In the remaining 21 h, the temperature in the freezing pipe was increased.

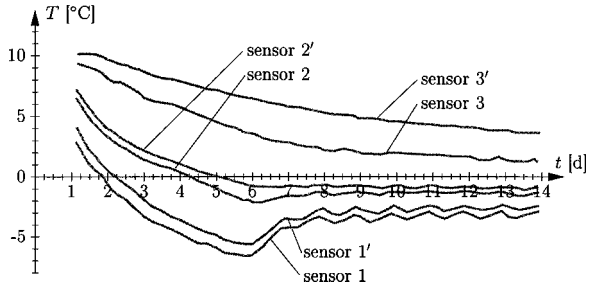

Fig. 13. Application: temperature histories at temperature sensors measured at construction site

Since no temperature history of the brine material is available, a linear decrease from 10 to −30°C is assumed during the first day of the first part of the freezing process (see Fig. 14). A similar temperature history is reported in Deix (1992). In the course of intermittend freezing, abrupt changes of the temperature between the freezing temperature of −30°C (3 h/day) and −5°C (21 h/day) are assumed. The temperature level of −5°C is based on the requirement that the soil temperature in the center of the frozen-soil body should always be lower than −5°C. The temperature history employed in the numerical analysis is shown in Fig. 14.

Material Properties

According to Deix (1992), the frozen soil body of test Field V2 is located in a gravel/sand layer. The two soil-specific material parameters required as input for the proposed phase-change model, f_p and $f_{i,\infty}$, are obtained as

1. The volume fraction of the soil particles f_p is determined from the water content $w=0.20$ given in Deix (1992) using

$$w = \frac{f_w \rho_w}{f_p \rho_p} = \frac{(1-f_p)\rho_w}{f_p \rho_p} \rightarrow f_p = \frac{\rho_w}{w\rho_p + \rho_w} = \frac{1{,}000}{0.20 \cdot 2650 + 1{,}000} = 0.65 \quad (15)$$

   where ρ_p and ρ_w were taken from Table 2.
2. The final volume fraction of ice is given by

$$f_{i,\infty} = f_w \frac{w_{f,\infty}}{w} = 0.33 \quad (16)$$

   where $w_{f,\infty}=0.19$ was obtained from setting $w-w_{f,\infty}$ equal to 0.01 (see Fig. 2).

Based on the material parameters of the different material phases (Table 2) and the given values of f_p and $f_{i,\infty}$, the thermal material properties for freezing soil are determined from Eqs. (7)–(9). In the following thermal analysis, the parameter $\bar{T}$ of the thermal freezing function is set equal to 0.2°C. Moreover, a released energy in consequence of freezing of $\ell_\xi=100{,}631$ kJ/(m^3 soil) is considered [Eq. (10)].

Finite Element Model: Initial and Boundary Conditions

In the numerical analysis, a two dimensional (2D) model representing the cross section of test Field V2 is employed. Because of the geometric dimensions of the test field (length × width × height = 30 m × 9 m × 1 m), the use of a 2D model is appropri-

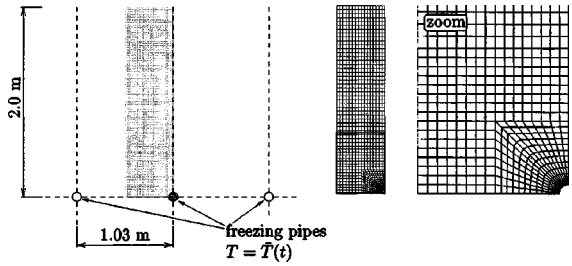

Fig. 15. Application: numerical model and finite-element discretization

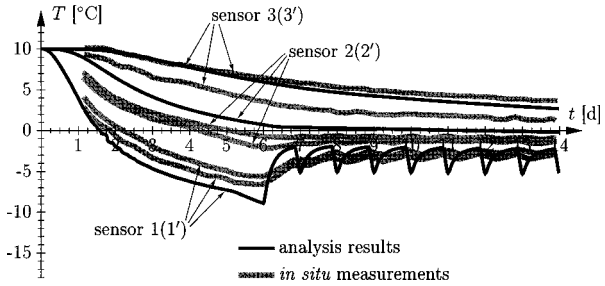

Fig. 16. Application: evolution of temperature at sensors 1(1′), 2(2′), and 3(3′)

ate. Within the cross section of test Field V2, the periodic arrangement of the freezing pipes was exploited by considering only the part of the test field containing the temperature sensors. Accounting for symmetry conditions, the final analysis model consists of one quarter of the freezing pipe and the surrounding soil. It has a width of $1.03/2 = 0.515$ m (see Figs. 12 and 15). Based on measurement data provided by the construction site, reporting a thickness of the frozen-soil body of approximately 1 m, the height of the numerical model was chosen as 2 m. Hence, only the lower part of the numerical model is expected to freeze during the analysis.

The initial temperature of the soil T_0 is set equal to 10°C. During freezing, the temperature history depicted in Fig. 14 is prescribed at the FE nodes at the boundary representing the quarter of the freezing pipe. At the remaining boundaries, the normal temperature flux q_n is set equal to zero (adiabatic conditions).

Presentation of Results

Fig. 16 shows the numerically obtained evolution of the temperature at the location of the temperature sensors. In view of the low number of soil-specific input parameters [water content w taken from Deix (1992) and $w_{f,\infty}$ obtained from Fig. 2], the numerical results agree rather well with the in situ measurements. During the first part of the freezing process, the temperature at the sensor 2(2′) is overestimated, whereas lower temperatures are predicted close to the freezing pipe at the sensor 1(1′). The numerically obtained temperature history at the sensor 3(3′) fits within the in situ measurements of sensor 3 and sensor 3′. For the second part of the freezing process, i.e., for intermittend freezing, the numerically obtained temperature history at sensor 1(1′) is characterized by higher freezing and thawing rates, resulting in larger oscillations of the temperature. This is explained by the abrupt changes of the temperature in the freezing pipe between the two temperature levels during intermittend freezing, i.e., between −5 and −30°C (see Fig. 14). At the construction site, on the other hand, the change from one temperature level to the other requires some time and depends on the employed freezing equipment. Unfortunately, no information about the real temperature history in the freezing pipe was available which would have allowed us to specify the in situ temperature history for the cooling pipe more accurately.

An important aspect in soil freezing by means of freezing pipes is the closing time t_c, i.e., the time instant at which the frozen bodies which are developing around the different freezing pipes merge to form a connected body of frozen soil. Fig. 17 shows the location of the freezing front (0° isotherm) for different instants of time. The numerically obtained closing time t_c is 114 h. It refers to the time instant when the freezing front reaches the left boundary of the numerical model (see Fig. 15).

Standardly, analytical expressions are used for the estimation of the closing time t_c. Based on a constant brine temperature of −30°C from the beginning of freezing, the closing time t_c can be estimated according to Sanger and Sayles (1979)

$$t_c = \frac{R^2 L}{4k(\xi=1)\cdot(T_f-\overline{T})}\left(2\cdot\ln\frac{R}{r}-1+\frac{\rho(\xi=1)\cdot c(\xi=1)\cdot(T_f-\overline{T})}{L}\right) = \frac{0.515^2\times 200{,}213}{4\cdot 15.7\times(0+30)}\left(2\cdot\ln\frac{0.515}{0.032}-1+\frac{2{,}012\times 0.96\cdot(0+30)}{200{,}213}\right)$$
$$= 137 \text{ h} \tag{17}$$

with

$$L = \ell_\xi + \frac{a_r^2-1}{2\cdot\ln a_r}\cdot\rho(\xi=0)\cdot c(\xi=0)\cdot(T_0-T_f)$$
$$= 100{,}631 + \frac{3^2-1}{2\cdot\ln 3}\cdot 2072\times 1.32\cdot(10-0)$$
$$= 200{,}213 \text{ kJ/m}^3 \tag{18}$$

The analytical expression for the closing time given in Eq. (17) was derived under the assumption of axisymmetric conditions. Hence, no interaction between adjacent freezing pipes is taken into account. Accordingly, even though an abrupt decrease of the brine temperature to −30°C was assumed in Eq. (17), which should yield an underestimation of the closing time, disreporting the interaction between adjacent freezing pipes results in an overestimation of the closing time t_c by the analytical solution by Sanger and Sayles (1979).

Whereas the thickness of the frozen-soil body increases continuously during the first part of the freezing process, it should remain constant during intermittend freezing. During the latter, the frozen-soil body should have a minimum thickness in order to provide sufficient support for the excavation work. On the other

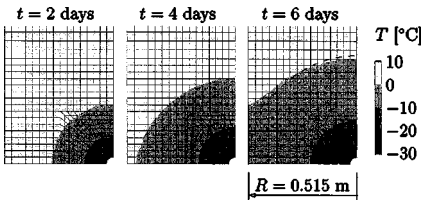

Fig. 17. Application: numerically obtained temperature distribution for different instants of time

hand, the thickness should be as small as possible in order to minimize the effect of frost heave and, hence, damage of surface buildings. Fig. 18 shows the evolution of the thickness of the frozen-soil body taken as the vertical distance between the −1°C isotherm at the upper and the lower side of the frozen-soil body. The evolution of the thickness of the frozen-soil body is plotted for at three different locations: at the left boundary of the numerical model (minimum thickness $d_{\min}$), at the right boundary of the numerical model (maximum thickness $d_{\max}$), and at the location of the vertical borehole containing the temperature sensors (d_{sensor}). According to the numerical results, a frozen-soil body with a thickness ranging from 0.5 (minimum thickness) to almost 1.0 m (maximum thickness) is built up during the first part of the freezing process. The size of the frozen-soil body continues to increase during intermittend freezing. This is in accordance with in situ observations at the location of the temperature sensors (compare in situ measurements in Fig. 18 with evolution of d_{sensor}). In fact, this result of test Field V2 was considered during the remaining freezing work at the construction site. The freezing time characterized by a brine temperature of −30°C was reduced from 3 to $1\frac{1}{2}$ h/day during intermittend freezing.

Parameter Study

In this study, the effect of design parameters of intermittend freezing on the thickness of the frozen-soil body is investigated. As mentioned before, the time span characterized by a temperature in the freezing pipe of $\overline{T}=-30°\text{C}$ (in the following denoted as Δt) may be changed. Additionally, the upper temperature level which was set equal to −5°C (in the following denoted as $\overline{T}_{\max}$) may be modified.

Fig. 19 shows the evolution of the minimum thickness $d_{\min}$ of the frozen-soil body for $\Delta t=1$, 3, and 5 h/day and $\overline{T}_{\max}=-5°\text{C}$. The increase of Δt from originally 3 to 5 h/day resulted in anincrease of the growth rate of the frozen-soil body. The reduction of

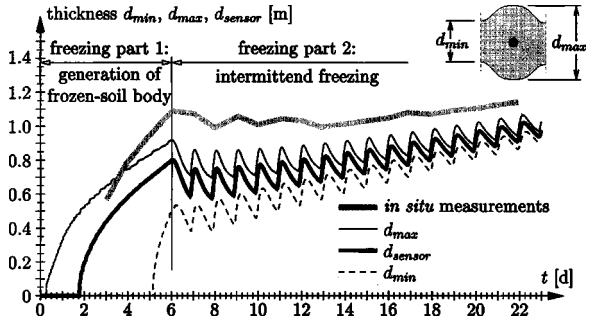

Fig. 18. Application: numerically obtained evolution of thickness of frozen-soil body characterized by $T\leqslant -1°\text{C}$

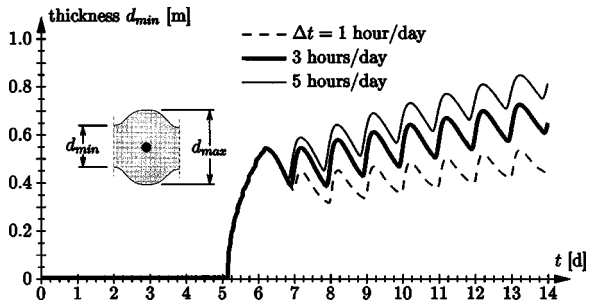

Fig. 19. Application: evolution of $d_{\min}$ for different time spans Δt and $\overline{T}_{\max}=-5°\text{C}$

Δt, on the other hand, caused a decrease of $d_{\min}$ right after the start of intermittend freezing, followed by a slight increase of $d_{\min}$. The obtained results support the decision of the freezing crew to reduce Δt from 3 to 1.5 h/day. This provided the minimum thickness required as structural support by an almost constant evolution of $d_{\min}$ during intermittend freezing.

The influence of the upper temperature level $\overline{T}_{\max}$ on the thickness of the frozen-soil body is illustrated in Fig. 20. A reduction of $\overline{T}_{\max}$ from −5 to −10°C led to an increase of the growing rate of the thickness of the frozen-soil body by a factor of 2. The increase of $\overline{T}_{\max}$ to 0°C, on the other hand, resulted in the separation of the frozen-soil body. During the construction process, such a situation must be avoided. If the frozen-soil body becomes disconnected, it loses its structural effect and, hence, may cause collapse of the support system.

Influence of Latent Heat of Freezing

Finally, the influence of the energy release in consequence of freezing, ℓ_ξ, on the numerical results is assessed by an additional analysis. Setting ℓ_ξ equal to zero led to a significant underestimation of the temperature history at all temperature sensors (Fig. 21). In the first part of the freezing process, the minimum thickness $d_{\min}$ of the frozen-soil body increases up to 2 m (see Fig. 22). During intermittend freezing, $d_{\min}$ remains almost constant. However, at $t=10$ days a further increase of $d_{\min}$ is observed. This is a consequence of boundary effects of the numerical model. For the size of the frozen-soil body predicted by the analysis disregardingthe influence of the latent heat of freezing, the height of the numerical model needs to be increased.

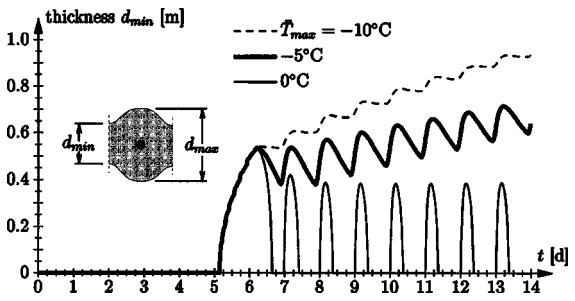

Fig. 20. Application: evolution of $d_{\min}$ for different temperature levels $\overline{T}_{\max}$ and $\Delta t=3$ h

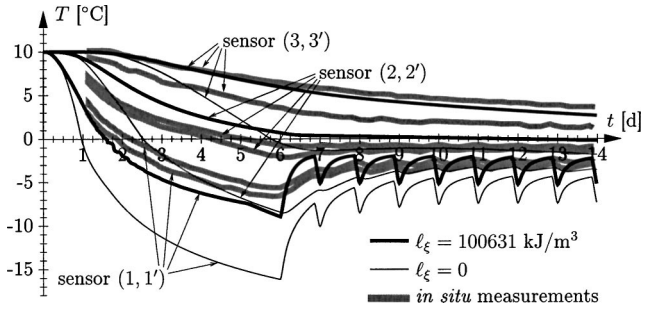

Fig. 21. Application: influence of latent heat ℓ_ξ on evolution of temperature history at sensors $1(1')$, $2(2')$, and $3(3')$

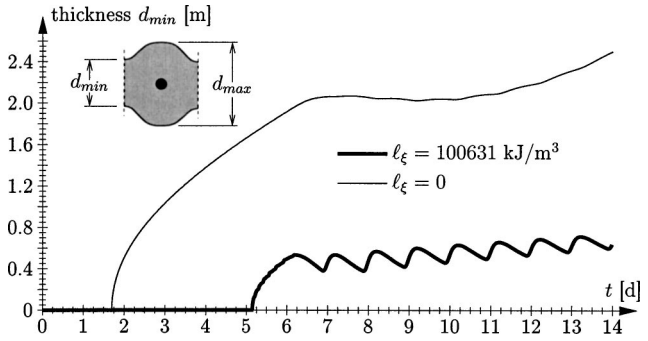

Fig. 22. Application: influence of latent heat ℓ_ξ on evolution of minimum thickness $d_{\min}$ of frozen-soil body

Conclusions

This paper dealt with the development of a phase-change material for the description of the thermal problem of freezing of fully saturated soil. In order to minimize the number of input material parameters, the properties of freezing soil were derived by means of homogenization techniques employing parameters of the different material phases, such as water, ice, and soil particles. The unfrozen water content, which is commonly observed for soil cooled below the freezing temperature, was related to the temperature by a so-called thermal freezing function. Hereby, a new material parameter accounting for chemical bonds and electrostatic forces at the surface of the soil particles is introduced. In the course of reanalysis of freezing experiments recently performed at Vienna Univ. of Technology, this parameter was specified for fully saturated sand. Moreover, the reanalysis of the experiments revealed a good performance of the developed material model with regard to both cooling in the prefreezing and postfreezing regime and the time span corresponding to freezing of the specimen characterized by almost constant temperature.

Finally, the material model was employed for the simulation of on-site freezing work performed in the course of the construction of the Vienna underground system. From the obtained results, the following conclusions can be drawn:

1. Disregard of the enthalpy change in consequence of freezing resulted in an underestimation of the temperature history measured at the construction site. Moreover, the thickness of the frozen-soil body was significantly overestimated.
2. During intermittend freezing, the temperature in the freezing pipe is increased for 21 h/day from $\overline{T}=-30\,^\circ\mathrm{C}$ to a temperature level of $-5\,^\circ\mathrm{C}$. This temperature level was found to have strong impact on the evolution of the thickness of the frozen-soil body. Changing the time span characterized by a temperature in the freezing pipe of $\overline{T}=-30\,^\circ\mathrm{C}$, on the other hand, showed a moderate effect on the thickness of the frozen-soil body, being well-suited for fine-tuning the freezing work at the construction site.

The evolution of the thickness of the frozen-soil body is of essential importance during AGF. On the one hand, a minimum thickness should be provided in order to guarantee the required support during the excavation process. On the other hand, a too large or continuously increasing thickness of the frozen-soil body results in unwanted frost heave and, hence, in damage of the surface infrastructure. The developed phase-change model and the numerical simulations presented in this paper provided first insight into this optimization problem, aiming at a constant thickness of the frozen-soil body during intermittend freezing.

Acknowledgment

The writers want to thank Franz Deix (Magistratsdirektion, Stadtbaudirektion, Gruppe Tiefbau & Verkehr, Vienna, Austria) for the communication of monitoring data from the considered tunnel construction site.

Notation

The following symbols are used in this paper:

A = pre-exponential constant;
A_g = pre-exponential constant for crystal growth;
A_n = pre-exponential constant for local diffusion process;
a_r = parameter used in analytical solution for closing time, with $a_r=3$;
c = heat capacity;
c_i = heat capacity of ice;
c_p = heat capacity of soil particles;
c_w = heat capacity of water;
d = thickness of frozen-soil body;
f_i = volume fraction of ice;
$f_{i,\infty}$ = final volume fraction of ice for $T \ll T_f$;
f_p = volume fraction of soil particles;
f_w = volume fraction of water;
H = enthalpy;
k = thermal conductivity;
k_i = thermal conductivity of ice;
k_p = thermal conductivity of soil particles;
k_w = thermal conductivity of water;
L = parameter used in analytical solution for closing time;
ℓ_ξ = released energy of freezing;
m = mass of saturated soil sample;
m_p = mass of soil particles (dried soil sample);
m_w = mass of water;
Q = activation energy;
Q_g = activation energy of crystal growth;
Q_n = activation energy of local diffusion process;
q = heat flux;
q_n = normal heat flux;
R = radius of frozen-soil body in analytical solution; universal gas constant;
r = radius of freezing pipe;
S = scalar quantity representing Eshelby tensor;
T = temperature;

$\overline{T}$ = prescribed temperature in freezing pipe; constant reference temperature; calibration parameter in thermal freezing function;
T_f = freezing temperature;
$\overline{T}_{\max}$ = maximum temperature of prescribed temperature $\overline{T}$ during intermittend freezing;
T_0 = initial temperature of soil;
T^{∞} = temperature in cooling box;
t = time;
t_c = closing time;
V = volume of soil sample;
V_p = volume of soil particles;
V_w = volume of water;
w = water content;
w_f = frozen water content;
$w_{f,\infty}$ = final frozen water content for $T \ll T_f$;
α = radiation coefficient;
α, β = constant parameters in expression for nucleation rate;
ΔH = enthalpy change in consequence of freezing;
Δt = time span with $\overline{T} = -30\,^{\circ}\mathrm{C}$ during intermittend freezing;
ξ = degree of freezing;
ξ° = freezing rate;
ρ = density of soil;
ρ_i = density of ice;
ρ_p = density of soil particles;
ρ_w = density of water; and
τ_f = characteristic time of freezing process.

References

Atkins, P. W. (1994). *Physical chemistry*, 5th Ed., Oxford Univ. Press, Oxford, U.K.

Coussy, O. (1995). *Mechanics of porous continua*, Wiley, Chichester, U.K.

Deix, F. (1992). "Kombination setzungsmindernder und umweltschonender Massnahmen (Solevereisung, Druckluft, Ausbruchsicherung) beim innerstädtischen Tunnelbau in kritischen Bereichen," PhD thesis, Vienna Univ. of Technology, Vienna, Austria (In German).

Fletcher, N. (1970). *The chemical physics of ice*, Cambridge Univ. Press, Cambridge, U.K.

Gröber, H., Erk, S., and Grigull, U. (1988). *Die grundgesetze der wärmeübertragung*, 2nd Ed., Springer, Berlin (in German).

Häfner, F., Sames, D., and Voigt, H.-D. (1992). *Wärme- und stofftransport [heat and mass transport]*, Springer, Berlin (in German).

Hatta, H., and Taya, M. (1986). "Equivalent inclusion method for steady state heat conduction in composites." *Int. J. Eng. Sci.*, 24(7), 1159–1172.

Lackner, R., Blab, R., Jäger, A., Spiegl, M., Kappl, K., Wistuba, M., Gagliano, B., and Eberhardsteiner, J. (2004). "Multiscale modeling as the basis for reliable predictions of the behavior of multi-composed materials." *Progress in computational structures technology*, B. Topping and C. Mota Soares, eds., Saxe-Coburg, Chap. 8, Stirling, U.K., 153-187.

Lagger, H. (2001). "Ground improvement: ground freezing in tunneling." Ms thesis, Vienna Univ. of Technology, Vienna, Austria.

Mikkola, M., and Hartikainen, J. (2002). "Computational aspects of soil freezing problem." *Proc., 5th World Conf. on Computational Mechanics*, (CD ROM), H. Mang, F. Rammerstorfer, and J. Eberhardsteiner, eds., Vienna Univ. of Technology, Vienna, Austria.

Pitts, D., and Sissom, L. (1977). *Heat transfer*, McGraw-Hill, London.

Rolph, W. I., and Bathe, K.-J. (1982). "An efficient algorithm for analysis of nonlinear heat transfer with phase changes." *Int. J. Numer. Methods Eng.*, 18, 119–134.

Sanger, F., and Sayles, F. (1979). "Thermal an rheological computations for artificially frozen ground construction." *Eng. Geol. (Amsterdam)*, 13, 311–337.

Shackelford, J. (2000). *Materials science for engineers*, 5th Ed., Prentice-Hall, Upper Saddle River, N.J.

Willams, P. (2001). "Thermodynamic of mechanical conditions within frozen soil and their effects." *Proc., 5th Int. Conf. on Permafrost*, 493–498.